

Surfaces of the perovskite manganites $\text{La}_{1-x}\text{Ca}_x\text{MnO}_3$

Jaewu Choi

*Department of Physics and Astronomy and the Center for Materials Research and Analysis, Behlen Laboratory of Physics,
University of Nebraska-Lincoln, Lincoln, Nebraska 68588-0111*

Jiandi Zhang*

Solid State Division, MS-6057, Oak Ridge National Laboratory, Oak Ridge, Tennessee 37831-6030

S.-H. Liou and P. A. Dowben

*Department of Physics and Astronomy and the Center for Materials Research and Analysis, Behlen Laboratory of Physics,
University of Nebraska-Lincoln, Lincoln, Nebraska 68588-0111*

E. W. Plummer

*Solid State Division, MS-6057, Oak Ridge National Laboratory, Oak Ridge, Tennessee 37831-6030
and Department of Physics, University of Tennessee, Knoxville, Tennessee*

(Received 13 April 1998; revised manuscript received 19 November 1998)

Angle-resolved core-level photoemission has been utilized to study the surfaces of crystalline thin films of manganite $\text{La}_{1-x}\text{Ca}_x\text{MnO}_3$ ($x=0.1$ and 0.35). It is found that both the surface termination and Ca surface concentration depend on the bulk Ca concentration. For $\text{La}_{0.65}\text{Ca}_{0.35}\text{MnO}_3$, the terminal layer is predominately Mn-O, while for $\text{La}_{0.9}\text{Ca}_{0.1}\text{MnO}_3$, the majority of the surface is La/Ca-O terminated. Both surfaces exhibit a large enhancement in the Ca concentration compared to the bulk with the $\text{La}_{0.9}\text{Ca}_{0.1}\text{MnO}_3$ sample, having a larger surface Ca concentration than for the $\text{La}_{0.65}\text{Ca}_{0.35}\text{MnO}_3$ material. [S0163-1829(99)04420-3]

I. INTRODUCTION

The perovskite manganite $L_{1-x}A_x\text{MnO}_3$ family (L denotes lanthanide and A alkaline-earth doping ions) has attracted considerable attention because of their interesting electronic and magnetic properties.¹ For doping concentration $0.2 \leq x \leq 0.5$, these materials exhibit a paramagnetic to ferromagnetic phase transition with temperature, accompanied by a nonmetal-to-metal transition. The transport properties can be strongly influenced by an external magnetic field, thus resulting in the appearance of a negative colossal magnetoresistance behavior around the Curie temperature (T_C). Epitaxial thin films and heterostructures of these materials may find applications due to a rich array of electrical, magnetic, and optical properties.² However, when films are made thinner and thinner, the lattice structure and chemical composition on the surface and at the interface will play an important role in the electronic and magnetic properties. Thus the properties of epitaxial thin films may be significantly different from the corresponding bulk materials.³ Furthermore, many techniques used today such as angle-resolved and spin-resolved photoemission attempt to study the bulk by "looking the bulk through the surface."^{4,5} The surface-related properties will certainly mingle with truly bulk physics.

Different surface preparations could lead to different surface structure and stoichiometry, particularly for surfaces of complex materials. There are several methods used to obtain a clean surface. The first one (maybe the best way) is to cleave a single crystal *in situ*. Except for possible surface lattice relaxation or reconstruction, the surface composition

will resume the same as that of the bulk, especially at relatively low temperature. Unfortunately, not all single crystals of perovskite manganites can be cleaved due to their intrinsic three-dimensional structure. Another way to obtain a good surface of these compounds is to grow the crystalline films *in situ* with techniques like laser ablation, where, in principle, a surface with correct stoichiometry could be fabricated. In practice, surface segregation can occur because of high temperature during the growth of the films. Izumi *et al.*⁶ reported on the epitaxial growth of $\text{La}_{0.6}\text{Sr}_{0.4}\text{MnO}_3$ films where atomically smooth surfaces can be obtained using pulsed laser deposition. However, "dead layers" are also formed at interfaces and the properties for the thin films (with about 4-nm thickness) are considerably different from the thick films, indicating the influence of the surface and/or interface. The third way to obtain a clean surface of these compounds is through transporting thin films into a vacuum chamber and cleaning and processing in vacuum (as we employed in this study). This method was applied by Park *et al.*⁵ for the observation of the half-metallic character on the surface of $\text{La}_{0.6}\text{Sr}_{0.4}\text{MnO}_3$ films. McIlroy *et al.* also utilized the same method for their angle-resolved photoemission studies on the surfaces of $L_{1-x}A_x\text{MnO}_3$ films.⁴ In all cases, it is extremely important to determine the surface structure and stoichiometry before making any conclusion on the characterization of the bulk properties. In this paper we report our observations on the surface termination and surface composition of perovskite manganite $L_{1-x}A_x\text{MnO}_3$. We believe that these results should have profound impact on the implications of experiments using surface-sensitive techniques like photoemission to determine the bulk electronic structure.

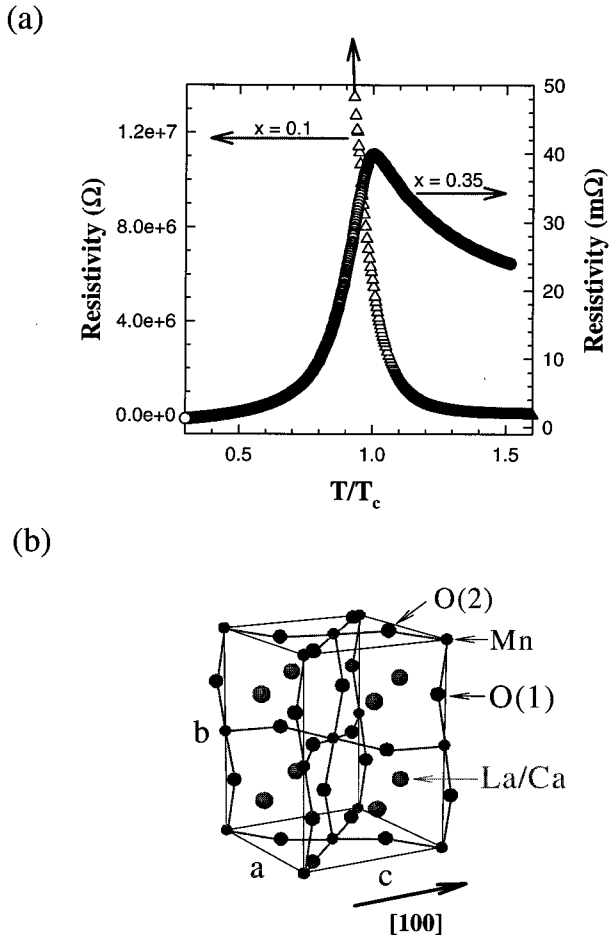


FIG. 1. The temperature dependence of the resistivity of $\text{La}_{1-x}\text{Ca}_x\text{MnO}_3$ [\triangle for $x=0.1$ ($T_c=150$ K), and \circ for $x=0.35$ ($T_c=260$ K)] films (a) and the schematic bulk unit cell with a distorted cubic perovskite (i.e., orthorhombic) structure (b). The crystal orientations in the ARXPS experiment are marked. The dramatic increase of the resistivity with decreasing temperature below T_c for $\text{La}_{0.9}\text{Ca}_{0.1}\text{MnO}_3$ is marked with an arrow along the data curve.

II. EXPERIMENTAL DETAILS

The $\text{La}_{1-x}\text{Ca}_x\text{MnO}_3$ ($x=0.1$ and 0.35) thin films were grown on (100) LaAlO_3 substrates by rf sputtering technique. The thickness of the samples is nominally 2500 \AA . The bulk chemical composition of the films was determined from energy dispersive analysis of x-ray emission spectroscopy, and found to be similar to the bulk targets with final compositions: $\text{La}_{0.9}\text{Ca}_{0.1}\text{MnO}_3$ and $\text{La}_{0.65}\text{Ca}_{0.35}\text{MnO}_3$. The quality of films was characterized by the measurements of its bulk properties such as the resistivity and magnetization as a function of temperature. As shown in Fig. 1(a), the temperature dependence of resistivity of the $\text{La}_{0.9}\text{Ca}_{0.1}\text{MnO}_3$ films shows insulating behavior, while the $\text{La}_{0.65}\text{Ca}_{0.35}\text{MnO}_3$ films undergo a metal to insulator transition around the Curie temperature of 260 K (T_c). The crystallinity and orientation were established by x-ray diffraction, and later by low-energy electron diffraction (LEED). Samples were cleaned by repeated annealing at 760 K and/or exposure to low energy electrons to stimulate the desorption of contaminants as

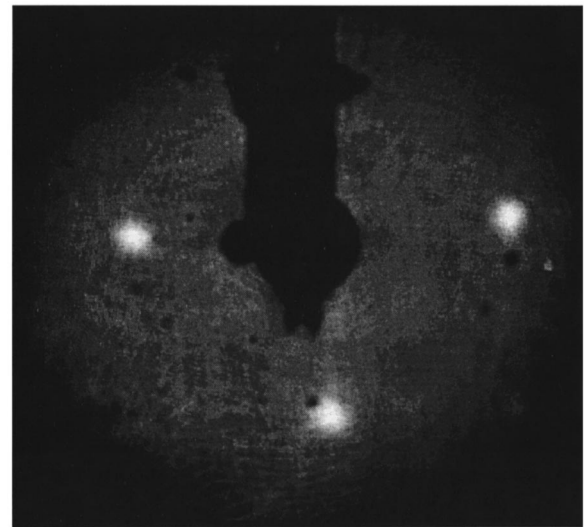


FIG. 2. The LEED pattern with an electron impact energy of 31 eV from the surface of $\text{La}_{0.65}\text{Ca}_{0.35}\text{MnO}_3$ at room temperature.

described elsewhere.⁴ The UHV chambers used for core level photoemission and electron energy-loss spectroscopy were maintained at a vacuum less than 2×10^{-10} Torr.

X-ray photoemission spectroscopy (XPS) was undertaken with the $\text{Mg-K}\alpha$ line (1253.6 eV) from a fixed anode x-ray source. Energy distribution curves of the elemental core levels were acquired with a hemispherical electron energy analyzer. The results were independent of pass energy, and therefore resolution. The binding energy of core levels are reported with respect to the Fermi level established from a tantalum foil in electrical contact with the sample. All the core-level data reported herein were taken at room temperature. Exposing the sample to oxygen during the annealing (at $450\text{--}500 \text{ }^\circ\text{C}$) and at room temperature did not change the LEED pattern and the XPS spectra as compared with those without oxygen treatment, suggesting that there is a stable surface oxygen stoichiometry though the absolute oxygen concentration is still unknown. For each bulk Ca concentration (i.e., $x=0.1$ and 0.35), several samples were measured, and it was found that the results were sample-independent.

The bulk lattice structure has been determined by the neutron-scattering experiments.⁷ As shown in Fig. 1(b), the bulk unit cell reveals a distorted cubic perovskite (i.e., orthorhombic) structure with a $Pnma$ space group symmetry. With x-ray-diffraction and LEED experiments, we found that the b axis of the bulk unit cell [Fig. 1(b)] is parallel to the surface normal in our crystalline thin films such that the surface plane is the (010) plane, i.e., the ac plane. Figure 2 shows the LEED picture from the surface of $\text{La}_{0.65}\text{Ca}_{0.35}\text{MnO}_3$ film. The square LEED pattern, though fuzzy, supports the conclusion on the film orientation obtained from x-ray diffraction. At this stage, we do not know the details of the surface relaxation, only that the surface is not reconstructed.

III. DETERMINATION OF THE TERMINAL LAYER

Though the surface of $\text{La}_{1-x}\text{Ca}_x\text{MnO}_3$ ($x=0.1$ and 0.35) films is terminated with the ac plane, there are at least three possible termination ways: either a Mn-O or La/Ca-O layer, or a mixture of them. In order to determine the surface ter-

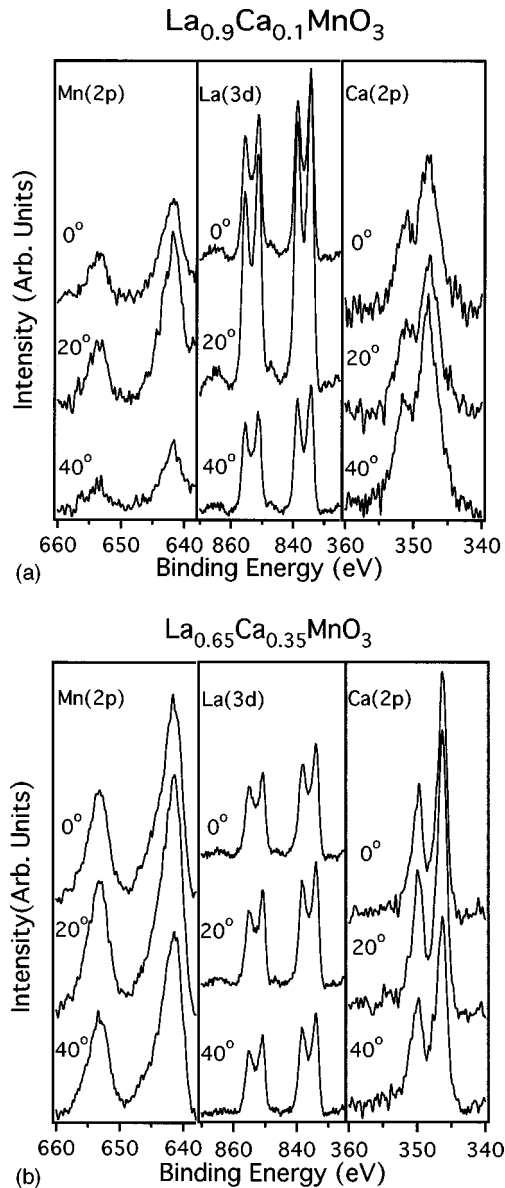


FIG. 3. Selected core-level photoemission spectra of (a) Mn $2p$, (b) La $3d$, and (c) Ca $2p$ states, at three different emission angles 0° , 20° , and 40° with respect to the surface normal, for $\text{La}_{0.9}\text{Ca}_{0.1}\text{MnO}_3$ (a) and $\text{La}_{0.65}\text{Ca}_{0.35}\text{MnO}_3$ (b).

mination layer, we have investigated the angular dependence of the core-level intensity ratio from the surfaces of these two compounds. The La $3d$, Mn $2p$, and Ca $2p$ core-level spectra as functions of emission angle with respect to the surface normal are shown in Fig. 3(a) for $\text{La}_{0.9}\text{Ca}_{0.1}\text{MnO}_3$ and Fig. 3(b) for $\text{La}_{0.65}\text{Ca}_{0.35}\text{MnO}_3$. There are some noticeable and quantitative differences in the angular intensities in Fig. 3. The most striking feature is in the Ca ($2p$) core level, where for the $\text{La}_{0.9}\text{Ca}_{0.1}\text{MnO}_3$ sample the intensity significantly increased at 40° compared to the data for $\text{La}_{0.65}\text{Ca}_{0.35}\text{MnO}_3$. In an attempt to quantify the core-level behavior, in Fig. 4 we plot the normalized core-level intensity ratio of the Mn ($2p_{1/2}$ and $2p_{3/2}$) and the Ca ($2p_{1/2}$ and $2p_{3/2}$) plus La ($3d_{3/2}$ and $3d_{5/2}$). Each core level was normalized with respect to its relative cross section.⁸ Figure 4 shows that the two surfaces are fundamentally different, with the Mn intensity relative to the La+Ca being considerably

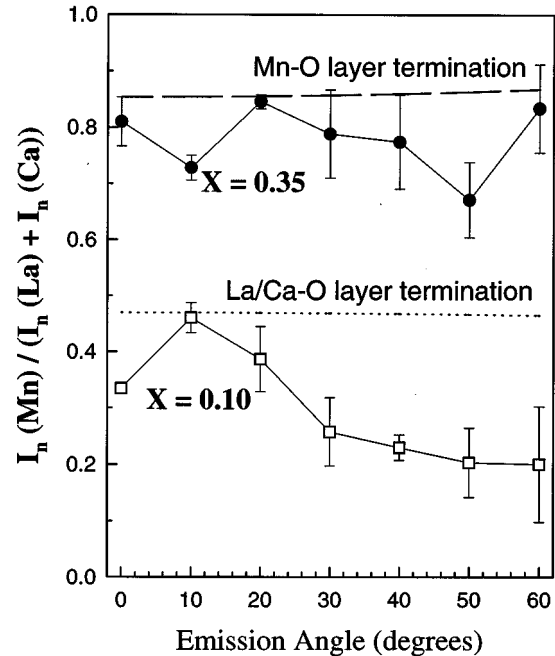


FIG. 4. The normalized core-level intensity ratio of Mn to La-Ca, $I_n(\text{Mn})/[I_n(\text{La})+I_n(\text{Ca})]$ as a function of emission angle for $\text{La}_{0.9}\text{Ca}_{0.1}\text{MnO}_3$ and $\text{La}_{0.65}\text{Ca}_{0.35}\text{MnO}_3$. The calculated results of the intensity ratio with either a Mn-O (dashed line) or La/Ca-O (dotted line) terminal layer are also presented.

higher for the $x = 0.35$ sample than for the $x = 0.1$ Ca sample. The relative cross sections for this photon energy predicted from simple calculations with either Mn-O or La/Ca-O layer termination are shown in Fig. 4 for comparison. The cross sections for Mn-O layer termination are calculated for $x = 0.35$ Ca doping, while the cross sections for La/Ca-O layer termination are calculated for $x = 0.1$ Ca doping. Though these calculations are based upon that assumption that there is no Ca surface segregation, the correction for the segregation, as discussed below, only reinforces our termination assignment in the model calculations. Based on a comparison between the model calculations and experimental results, it is clear that surfaces of these two compounds have different terminations. For $\text{La}_{0.65}\text{Ca}_{0.35}\text{MnO}_3$ the dominant terminal layer is Mn-O while for $\text{La}_{0.9}\text{Ca}_{0.1}\text{MnO}_3$ it is mostly La/Ca-O terminated. For thin films of $\text{La}_{0.6}\text{Sr}_{0.4}\text{MnO}_3$ which has a similar doping level to $\text{La}_{0.65}\text{Ca}_{0.35}\text{MnO}_3$, Izumi *et al.* also observed that the surface is terminated with a Mn-O layer using coaxial impact collision ion-scattering spectroscopy.⁶ In Sec. IV we will demonstrate the presence of preferential Ca segregation to the surface.

A comparison of the oxygen $1s$ spectra from $\text{La}_{0.9}\text{Ca}_{0.1}\text{MnO}_3$ and $\text{La}_{0.65}\text{Ca}_{0.35}\text{MnO}_3$ to the oxygen spectra from the MnO surface, shown in Fig. 5, also supports our assignment for the termination. In contrast to the single O $1s$ core level of $\text{La}_{1-x}\text{Ca}_x\text{MnO}_3$; one at around 529 eV, and the other at about 531.4 eV. The existence of the two features reflects the chemical shifts in the oxygen core level due to two kinds of chemical environment: one associated with Mn-O bonding, and the other associated with La/Ca-O bonding (or defects). Since the lower-binding-energy feature (i.e.,

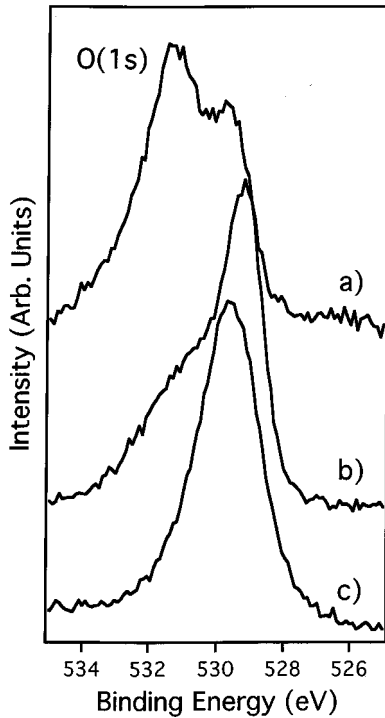


FIG. 5. O 1s core-level photoemission spectra from (a) $\text{La}_{0.9}\text{Ca}_{0.1}\text{MnO}_3$, (b) $\text{La}_{0.65}\text{Ca}_{0.35}\text{MnO}_3$, and (c) MnO (taken from Ref. 9). The spectra are compared for normal emission.

the 529-eV one) most closely resembles the binding energy (529.6 eV) of the O 1s core level in MnO ,⁹ we conclude that this peak is associated with the oxygen O(2) emission [see Fig 1(b)] with Mn-O bonding. The other one, with higher binding energy, is related to the oxygen O(1) emission [see Fig 1(b)]. In the $\text{La}_{0.65}\text{Ca}_{0.35}\text{MnO}_3$ sample, this lower-binding-energy O 1s state is more intense than the higher-binding-energy peak, indicating that the surface is primarily composed of a Mn-O bonding environment. On the other hand, in the $\text{La}_{0.9}\text{Ca}_{0.1}\text{MnO}_3$ sample, the reverse is true: the higher-binding-energy state has a greater intensity than the lower-binding-energy state, indicating that the surface is composed of a La/Ca-O bonding environment (or defects).

IV. SURFACE SEGREGATION

One can make use of the finite electron mean free path to determine the preferential segregation of one chemical component.¹⁰⁻¹² In photoelectron spectroscopy, the mean free path of a photoelectron from a certain core level can be changed with its kinetic energy by altering its incident photon energy. On the other hand, the effective mean free path normal to the surface (i.e., the probe depth by photoemission) can also be altered by changing the emission angle. In principle, the elemental concentrations can be determined by an analysis of the core-level photoelectron spectrum from each element as a function of either emission angle or photon energy. Here the method of changing the emission angle (θ) has been utilized.^{10,11}

Relative surface concentration for a binary alloy (A_xB_{1-x}) can be determined from the intensity ratio between the components of the alloy, where the intensity is normalized by the cross section (σ_A, σ_B) of the core level of each

element A and B . The normalized intensity ratio is given by

$$R(\theta) = \frac{I_A(\theta)/\sigma_A}{I_B(\theta)/\sigma_B}, \quad (1)$$

where θ is the emission angle with respect to the surface normal. From the normalized intensity ratio, the apparent surface concentration of element A is given by

$$C(\theta) = \frac{R(\theta)}{1 + R(\theta)}. \quad (2)$$

A summation should be undertaken to account for each layer contributing to the photoemission signal. Assuming surface segregation of component A occurs, and the segregation decays into the bulk monochromatically, an exponential profile is assumed because this is the most reasonable expectation for the variation of the free energy from the surface to the bulk.^{11,12} Thus the atomic fraction of component A at the j th layer below the surface is written as

$$f_j = \mathbf{x} + \delta \cdot e^{-j/G}, \quad (3)$$

where the parameters \mathbf{x} , δ , and G are the bulk fraction for element A , the segregation at the topmost layer and the segregation depth in units of the distance d between layers, respectively. Since the intensity is directly proportional to the elemental composition, Eq. (1) can be rewritten as

$$R(\theta) = \frac{\sum_{j=0}^{\infty} f_j e^{-j/\lambda_A(\theta)}}{\sum_{j=0}^{\infty} (1-f_j) e^{-j/\lambda_B(\theta)}} \quad [\lambda_{A,B}(\theta) = \lambda_{A,B}^0 / \cos \theta], \quad (4)$$

where λ_A^0 , and λ_B^0 are the effective mean free paths (in units of d , the distance between layers) for photoelectrons emitted from the particular core level, for components A and B , respectively.

The mean free path of the electron in the material were taken from the calculated mean free paths from Penn.¹³ Accounting for the different photoelectron kinetic energies of the pertinent from Ca 2p (897–902 eV) and La 3d (393–416 eV) core levels, with a Mg- $K\alpha$ line x-ray (1253.6 eV), mean free paths of 6.5 Å for La core levels and 12 Å for Ca core levels were used. Each core level was normalized with respect to its relative cross section.⁸ We also assume that the surface lattice structure and lattice constants are the same as those in the bulk, as determined from neutron and x-ray diffraction, such that the layer spacing $d = 1.96$ Å.

In addition, as the terminal layer is different for each Ca composition, $x = 0.1$ and 0.35, we have accounted for the need to sum beginning with a different terminal layer. For $\text{La}_{0.9}\text{Ca}_{0.1}\text{MnO}_3$, applying the analysis of Eqs. (1)–(4), we have assumed the terminal layer is the La/Ca-O layer, while for $\text{La}_{0.65}\text{Ca}_{0.35}\text{MnO}_3$, the terminal layer is the Mn-O layer. For example, $\text{La}_{0.9}\text{Ca}_{0.1}\text{MnO}_3$ has a superlattice structure with an order of La/Ca-O, Mn-O, La/Ca-O, and Mn-O layers at the first, second, third, and fourth layers, respectively.

For $\text{La}_{0.9}\text{Ca}_{0.1}\text{MnO}_3$, the summation with respect to layers in Eq. (4) is done over $2n$ for Ca and La, instead of every

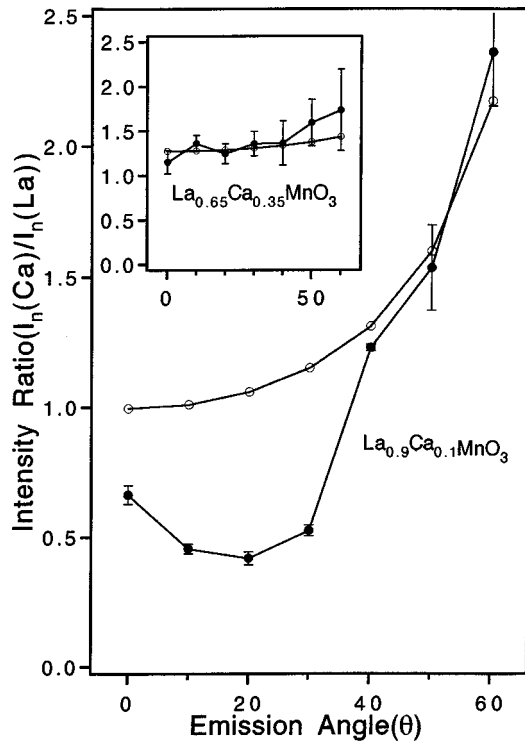


FIG. 6. The experimental normalized photoelectron intensity ratio of the Ca 2*p* and La 3*d* states as a function of emission angle for $\text{La}_{0.9}\text{Ca}_{0.1}\text{MnO}_3$ (●). The results are fitted assuming calcium segregation to the surface (see text) (○). In the inset, the normalized core-level intensity ratio of Ca 2*p* to La 3*d* state are shown for $\text{La}_{0.65}\text{Ca}_{0.35}\text{MnO}_3$ (●) together with a fitting that also assumes calcium surface segregation (○).

layer where n is positive integer which includes 0. This analysis was applied to XPS data with various emission angles as shown below:

$$R(\theta) = \frac{\frac{x}{1-\alpha} + \frac{\delta}{1-\alpha\gamma}}{\frac{1-x}{1-\beta} + \frac{\delta}{1-\beta\gamma}}, \quad (5)$$

where $\alpha = \exp[-2/\lambda_{\text{Ca}}(\theta)]$, $\beta = \exp[-2/\lambda_{\text{La}}(\theta)]$, and $\gamma = \exp(-2/G)$.

The angular dependence of the normalized intensity ratio of the photoelectron emitted from the La and Ca core levels are shown in Fig. 6. The results obtained from fitting the experimental data with Eq. (5) are also shown in this figure. For $\text{La}_{0.65}\text{Ca}_{0.35}\text{MnO}_3$, the normalized intensity ratio shows only small emission angle dependence, and the fitting is excellent using a small segregation ($\delta=0.24$) with segregation depth ($G=0.9$ layers). For $\text{La}_{0.9}\text{Ca}_{0.1}\text{MnO}_3$ the fitting is significantly worse, providing a segregation $\delta=0.82$ with segregation depth $G=0.4$ layers.

The poor fit for the $x=0.1$ sample at emission angles of about 20° can be explained by considering the effects of forward scattering.¹⁴⁻¹⁶ For the $\text{La}_{0.9}\text{Ca}_{0.1}\text{MnO}_3$ sample, the plane of incidence and emission is along the $\langle 010 \rangle$ plane [see Fig. 1(b)]. Given that the terminal layer is Ca-O, forward scattering by the La-O layers (separated by an Mn-O spacer layer in between) is anticipated, based upon geometrical con-

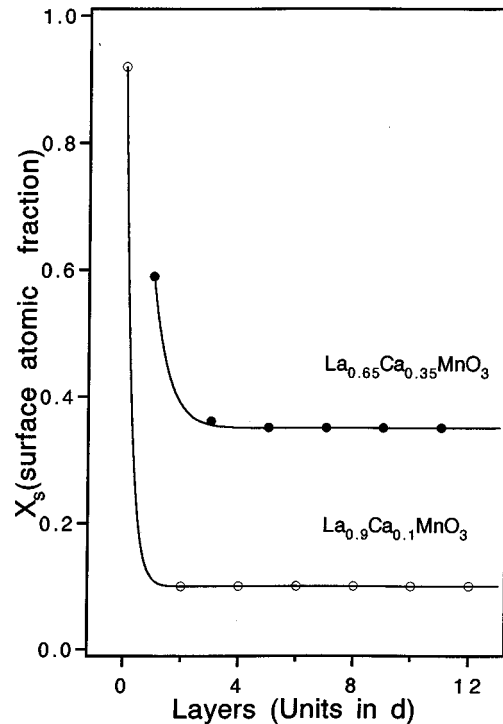


FIG. 7. Fitted Ca atomic fraction as a function of depth, in unit of d ($d=1.96 \text{ \AA}$), for both the $\text{La}_{0.9}\text{Ca}_{0.1}\text{MnO}_3$ and $\text{La}_{0.65}\text{Ca}_{0.35}\text{MnO}_3$. The La-Ca-O layers are the even layers for $\text{La}_{0.9}\text{Ca}_{0.1}\text{MnO}_3$, beginning with the terminal layer $d=0$, while, for the $\text{La}_{0.65}\text{Ca}_{0.35}\text{MnO}_3$ sample, the La/Ca-O layers are the odd-numbered layers beginning with the layer immediately below the surface ($d=1$).

siderations, at 19.5° . Thus, at this angle, the La signal from layers below, along this crystal plane, is expected to be greater than at other angles. Because of the large acceptance angle of our analyzer, the emission angle resolution in photoemission is degraded. Meanwhile, the forward scattering can also be degraded by surface disorder or imperfection (evident from fuzzy LEED pattern). Nonetheless, the expected forward-scattering effects are most pronounced around 20° off normal, close to the values expected from the bulk crystal structure. For $\text{La}_{0.65}\text{Ca}_{0.35}\text{MnO}_3$, the emission and incidence plane is along $\langle 110 \rangle$ [see Fig. 1(b)]. The intensity ratio between Ca and La is not effected, though a forward scattering of the Mn signal is expected, and observed (at around 43°).

According to the above fitting results, the Ca atomic fraction can now be plotted as a function of depth in units of layer d ($d=1.96 \text{ \AA}$), using Eq. (3), as shown in Fig. 7. For both samples, there is a considerable surface segregation. In particular, the surface of $\text{La}_{0.9}\text{Ca}_{0.1}\text{MnO}_3$ has an even more significant Ca segregation than that of $\text{La}_{0.65}\text{Ca}_{0.35}\text{MnO}_3$, indicating substantial differences in composition between the surface and bulk of these materials.

V. DISCUSSION

The surface Ca segregation is a strong indication that the surface enthalpy differs significantly from that of the bulk, in the context of standard statistical models. In a simple

statistical-mechanical model of segregation,¹⁷ the total free energy F for a system consisting of several elements is written as

$$F = \sum_i n_i^b g_i^b + n_i^s g_i^s - k_B T \ln \Omega, \quad (6)$$

where n_i^b and n_i^s are the number of bulk and surface atoms of type i with individual free energies g_i^b and g_i^s , respectively. Ω is the entropy due to the mixing of the compounds.

For a two-component system (an oversimplification to the La/Ca-O layers, admittedly), an Arrhenius expression is obtained:

$$n_1^s/n_2^s = n_1/n_2 \exp(-H/k_B T), \quad (7)$$

where H is the enthalpy of segregation.

Equation (6) implies that surface segregation is a competition to minimize the total free energy by a maximization of entropy by mixing evenly two elements and a minimization of free energy of each elements. From Eq. (7), the enthalpy can be determined as a function of the atomic fraction. The significant calcium segregation indicates that the surface of the $\text{La}_{1-x}\text{Ca}_x\text{MnO}_3$ samples is substantially different in the free enthalpy from the bulk-truncated surface. While a simple inspection of this statistical model does not provide the reason why the terminal layer has a calcium doping dependence, we are left with several conclusions.

First it is very clear that in the manganese perovskites, there is a very large driving force toward the equilibrium segregation of Ca: values of -50.3 kJ/mol for the heat of calcium segregation have been measured in magnesium oxide.¹⁸ When there is little significant segregation, the terminal layer is a polar surface—a surface is likely to be unstable toward surface reconstruction. These differences at the surface suggest that, under equilibrium conditions, the surface will not have a composition and/or structure representative of the bulk.

The fact that there is a large difference in free enthalpy between bulk and truncated surfaces without surface segregation means that *the surface could be fundamentally different from the bulk*. Even if there was a way to prepare a surface that resulted in an ideal bulk Ca concentration at the surface, the difference in free enthalpy would force the surface to be different electronically or structurally. Therefore, it would seem impossible to measure the bulk electronic properties using a surface-sensitive technique such as angle-resolved photoemission, especially in materials where the interlayer spacing is relatively larger than the mean free path of the photoexcited electron.

VI. CONCLUSION

This angle-resolved core-level photoemission study indicates, as should be expected, that the surface composition of $\text{La}_{1-x}\text{Ca}_x\text{MnO}_3$ is dramatically altered from its bulk. The surface termination layer depends on the Ca doping. For $x = 0.1$ doping, the terminal layer is the La/Ca-O layer, and, for $x = 0.35$, the terminal layer is the Mn-O layer. The existence of a preferential terminal layer, rather than termination in a random distribution of different layers, has also been observed from high- T_C superconducting materials like $\text{YBa}_2\text{Cu}_3\text{O}_{7-\delta}$ with ARXPS (Ref. 19) and Si-doped manganite with ion scattering spectroscopy.⁶ There is preferential Ca segregation to the surface, which is more dramatic for the low bulk doping ($x = 0.1$) than that for moderate bulk doping ($x = 0.35$), indicating a doping-dependent difference in the ratio of surface to bulk enthalpy.

ACKNOWLEDGMENTS

J.C., S.H.L., and P.A.D. were supported by NSF Grant No. DMR-98-02126/94-96131. J.D.Z. and E.W.P., were supported by the NEDO (JRCAT) of Japan and NSF Grant No. DMR-95-10132. Research at ORNL was sponsored by the Department of Energy managed by Lockheed Martin Energy Research Corp. under Contract No. DE-AC05-96OR22464.

*Present address: Department of Physics, Florida International University, Miami, FL 33199.

¹A. P. Ramirez, J. Phys.: Condens. Matter **9**, 8171 (1997), and references therein.

²Z. Trajanovic, C. Kwon, M. C. Robson, K.-C. Kim, M. Rajeswari, R. Ramesh, T. Vankatesan, S. E. Lofland, S. M. Bhagat, and D. Fork, Appl. Phys. Lett. **69**, 1005 (1996), and references therein; V. A. Vas'ko, V. A. Larkin, P. A. Kraus, K. R. Nikolaev, D. E. Grupp, C. A. Nordman, and A. M. Goldman, Phys. Rev. Lett. **78**, 1134 (1997).

³G. Gommert, H. Cerva, R. Rucki, R. Von Helmolt, J. Wecker, C. Kuhrt, and K. Samwer, J. Appl. Phys. **81**, 5496 (1996).

⁴D. N. McIlroy *et al.*, Phys. Lett. A **207**, 367 (1995); Jiandi Zhang *et al.*, Solid State Commun. **97**, 39 (1996); D. N. McIlroy *et al.*, Phys. Rev. B **54**, 17 438 (1996); Carlo Waldfried *et al.*, J. Phys. (Paris) **9**, 1031 (1997).

⁵J.-H. Park, E. Vescovo, H.-J. Kim, C. Kwon, R. Ramesh, and T. Venkatesan, Nature (London) **392**, 794 (1998); J.-H. Park, C. T. Chen, S.-W. Cheong, W. Bao, G. Meigs, V. Chakarian, and Y. U. Idzerda, Phys. Rev. Lett. **76**, 4215 (1996); A. Kay, E. Arenhols, S. Mun, F. J. Garcia de Abajo, C. S. Fadley, R. Denecke, Z. Hussain, and M. A. Van Hove, Science **281**, 679 (1998).

⁶M. Izumi, Y. Konishi, T. Nishihara, S. Hayashi, M. Shinohara, M. Kawasaki, and Y. Tokura, Appl. Phys. Lett. **73**, 2497 (1998); Wei Zhang, Xiaoru Wang, and Ian W. Boyd, *ibid.* **73**, 2745 (1998).

⁷See, e.g., E. O. Wollan and W. C. Koehler, Phys. Rev. **100**, 545 (1955); P. Dai, Jiandi Zhang, H. A. Mook, S.-H. Liou, P. A. Dowben, and E. W. Plummer, Phys. Rev. B **54**, R3694 (1996).

⁸J. H. Scofield, J. Electron Spectrosc. Relat. Phenom. **8**, 129 (1976).

⁹M. A. Langell, C. W. Hutchings, G. A. Carson, and M. H. Nassir, J. Vac. Sci. Technol. A **14**, 1656 (1996).

¹⁰Peter A. Dowben, in *Surface Segregation Phenomena*, edited by P. A. Dowben and A. Miller (CRC Press, Boston, 1990), 145.

¹¹Uresh Vahalia, Peter Dowben, and Allen Miller, J. Vac. Sci. Technol. A **4**, 1675 (1986).

¹²Uresh Vahalia, Peter Dowben, and Allen Miller, J. Electron Spectrosc. Relat. Phenom. **37**, 303 (1986).

¹³David R. Penn, J. Electron Spectrosc. Relat. Phenom. **9**, 29 (1976).

¹⁴W. F. Egelhoff, Jr., Surf. Sci. Rep. **6**, 253 (1987); S. Kono, S. M. Goldberg, N. F. T. Hall, and C. S. Fadley, Phys. Rev. B **22**, 6085 (1980).

- ¹⁵W. F. Egelhoff, Jr., Phys. Rev. B **30**, 1052 (1984); Phys. Rev. Lett. **59**, 559 (1987); R. A. Armstrong and W. F. Egelhoff, Jr., Surf. Sci. **154**, L225 (1985).
- ¹⁶W. F. Egelhoff, Jr., J. Vac. Sci. Technol. A **7**, 2060 (1989).
- ¹⁷S. Y. Liu and H. H. Kung, Surf. Sci. **110**, 504 (1981).
- ¹⁸Robert C. McCune and Paul Wynblant, J. Am. Chem. Soc. **66**, 111 (1983); W. C. Mackrodt and P. W. Tasker, J. Am. Chem. Soc. **72**, 1576 (1989); W. D. Kaplan *et al.*, *ibid.* **78**, 2841 (1995).
- ¹⁹G. Frank, Ch. Ziegler, and W. Göpel, Phys. Rev. B **43**, 2828 (1991); N. Terada, S. Ishibashi, M. Jo, M. Hirabayashi, H. Ihara, and S. Yamamoto, Appl. Phys. Lett. **63**, 2967 (1993).